Electronic Structure and Atomistic Computations for the interpretation of Synchrotron Experiments

Spectroscopy and microscopy

Lecture Focus:*Mainly Density Functional Theory (DFT-based) computations*

Nadia Binggeli

The Abdus Salam
International Centre for Theoretical Physics

Density-Functional Theory (DFT)

Total energy: $E[\rho]$

all ground-state properties determined by

Electronic density: $\rho(\vec{r})$

→ ρ *obtained by solving*

One-electron Schrödinger equation

(Kohn-Sham) :

$$H\phi_i(\vec{r}) = \varepsilon_i \phi_i(\vec{r})$$

For the N lowest energy states

$$\rho(\vec{r}) = \sum_{\varepsilon_i \le E_F} |\phi_i(\vec{r})|^2$$

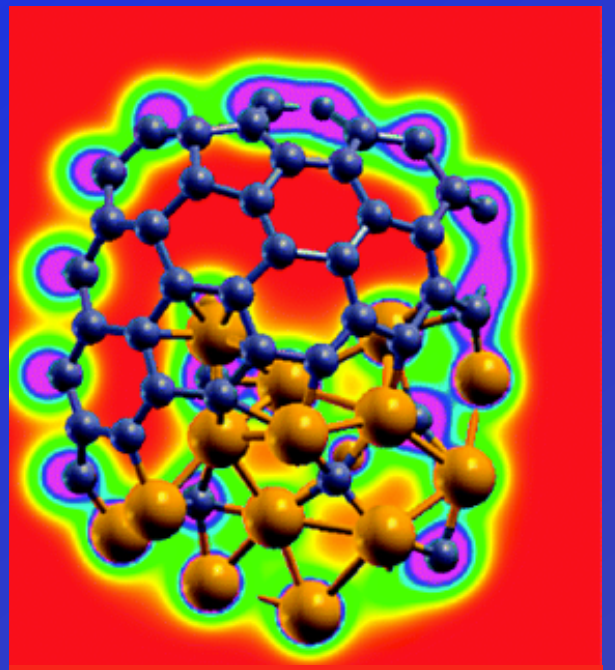

Nanotube cap on $Ni_{55}C_{14}$ Nanoparticles
Gomez-Ballesteros and Balbuena, ***Phys. Chem. Chem. Phys.***, **17**, 15056 (2015)

Density-Functional Theory (DFT)

Kohn-Sham DFT (Physical Review 1965)

(Use one-electron ϕ_i that reproduce true interacting ρ)

W. Kohn
Nobel 1998

L. J. Sham

One-electron Kohn-Sham equation:

$$\left\{-\frac{1}{2m_e}\nabla^2 + V_{nuc/ion}(\mathbf{r}) + V_C[\rho(\mathbf{r})] + V_{XC}[\rho(\mathbf{r})]\right\}\phi_i(\mathbf{r}) = \varepsilon_i\phi_i(\mathbf{r})$$

Periodicity
3D (crystal)
2D (surface)
1D (wire)
0D (molecule)

Functional
beyond.....
hybrid-GGA
GGA+U
GGA
LDA

TD-DFT
GW
GW+DMFT

Material modeling with DFT

Input

Atomic Structure or Composition

Output

Total Energy & Electronic Structure

Structural properties
atomic forces
equilibrium coordinates
atomic vibrations
phonons
stresses, pressure

Electronic properties
density of states
band structure
effect mass tensors
electron charge distribution
magnetism

Thermodynamics
internal energy (U)
enthalpy (H)
free energy (G)
activation energies (ΔE)

Excitations
transition intensities
dielectric functions
spectroscopy

From atomic aggregates to crystals

With periodic potential

$$\phi_{\vec{k}}(\vec{r}) = u_n(\vec{r})e^{i\vec{k}\cdot\vec{r}}$$

Bloch state

F. Bloch
1905-1983

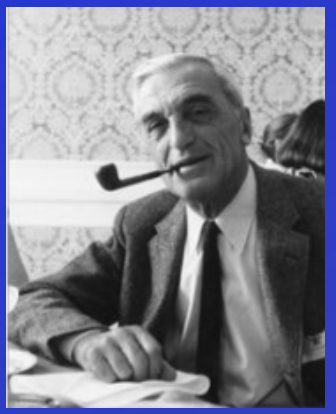

u: periodic (unit cell) part
k: wavevector in Brillouin zone

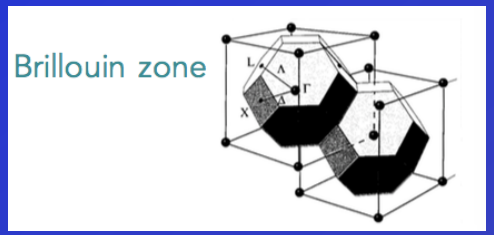

⟶ Band structure $\varepsilon(\vec{k})$

Electronic bulk band structure: Bulk Cu - GW compared to LDA

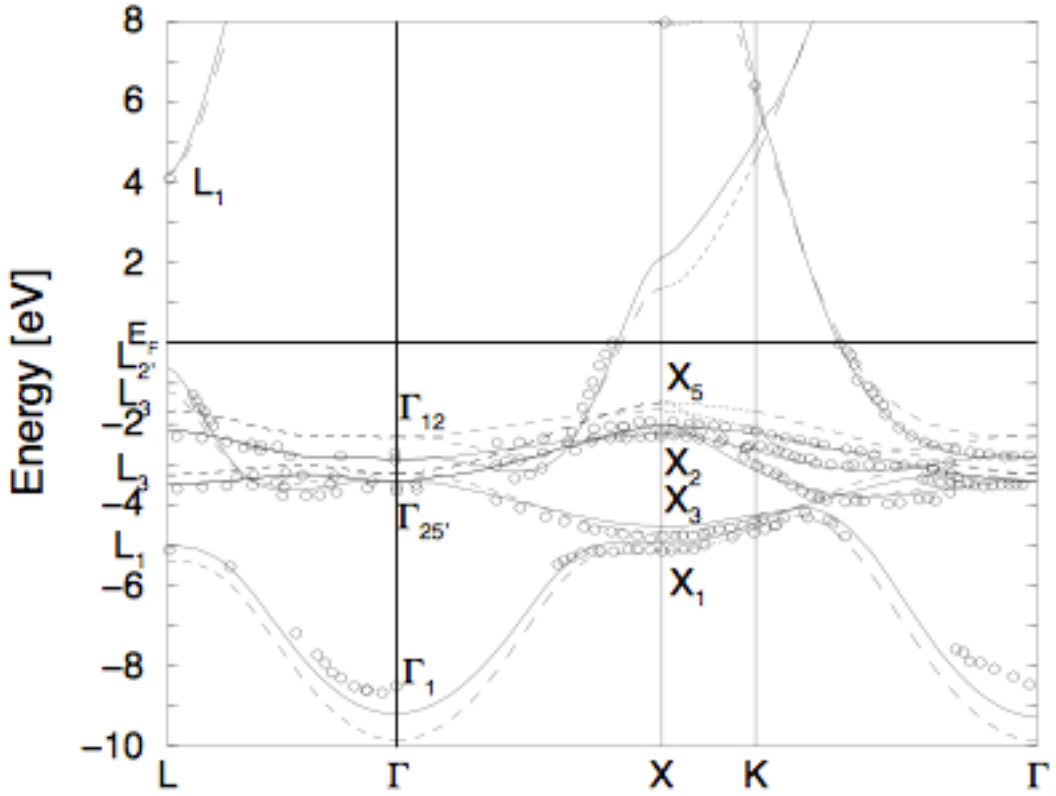

FIG. 2.: Full line: present GW results for the bulk copper band-structure, compared with the DFT–LDA results (dashed line), and with the experimental data reported in reference [16] (circles).

From: Andrea Marini, Giovanni Onida, and Rodolfo Del Sole, PRL **88**, 016403 (2001)

GW(solid line) best
LDA (dashed line) not bad

PS: Not always so:
strongly correlated materials

PE from:[16] R. Courths and S. Hufner, Phys. Rep. 112, 53 (1984)

Brillouin zone

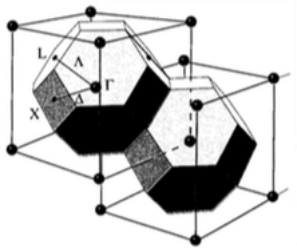

Electronic surface band structure
Si surface states – GW versus LDA

Surface states:

Si(100)-(2x1) surface

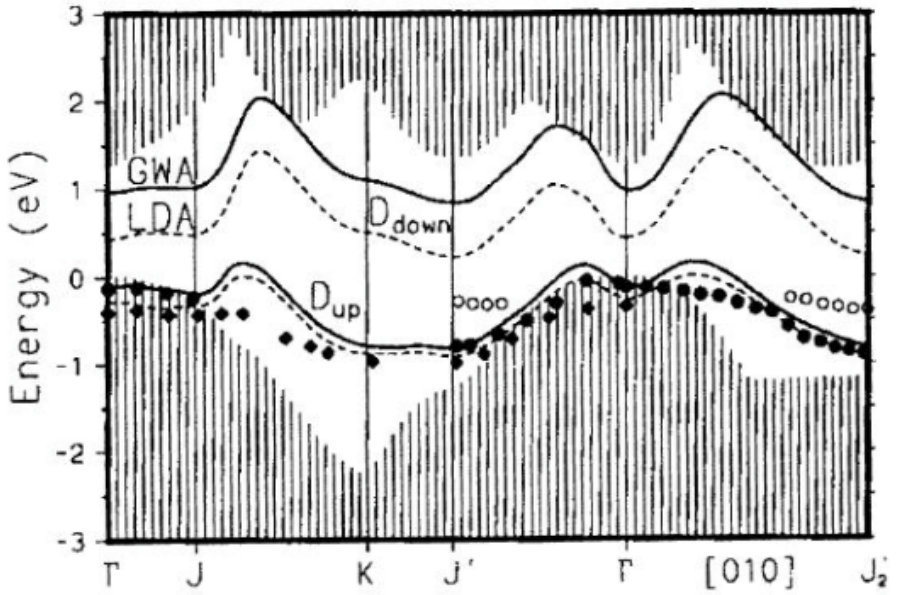

Figure 15. Calculated dangling-bond bands. Full curves, GWA energies; dashed curves, LDA energies. The experimental results are shown by diamonds (Uhrberg *et al* 1981) and circles (full and open) (Johansson *et al* 1990). (After Rohlfing *et al* 1995b).

Rohlfing, Krüger, and Pollmann, PRB 52, 1905 (1995)

Quantum-size effects on surface reactivity

Quantum-size effects are effects related to Quantum Well States (QWS), e.g., in ultrathin epitaxial films

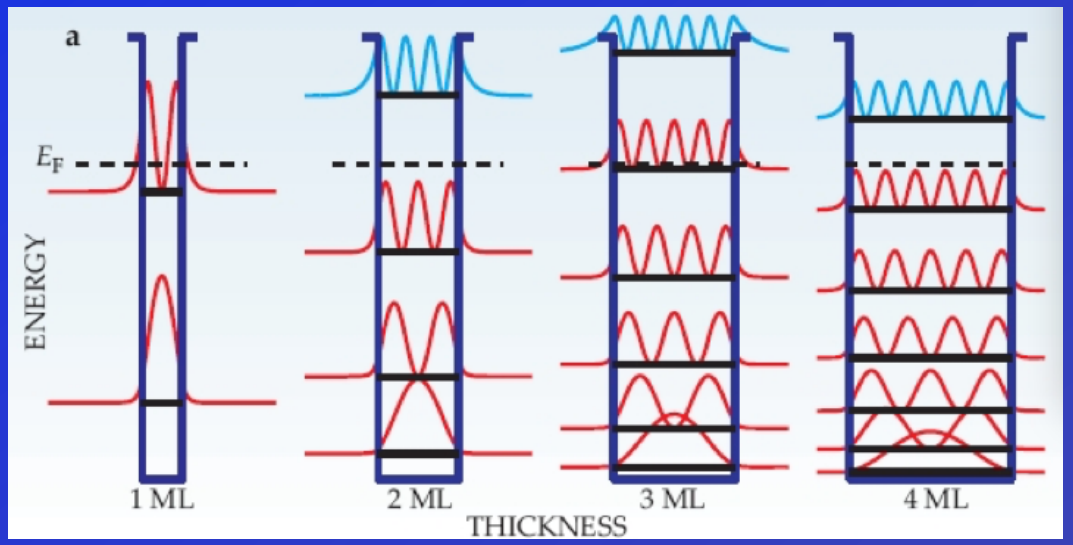

Observation of quantum well states

in thin metal films

By photoemission (PE): occupied QWS

Angle-resolved photoelectron spectroscopy

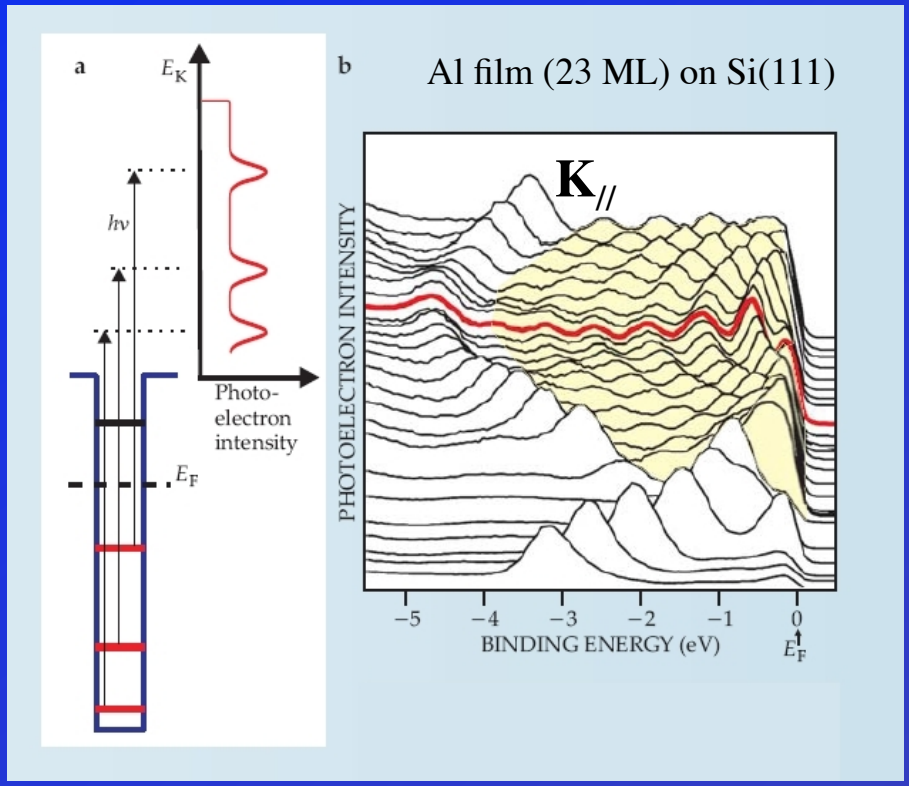

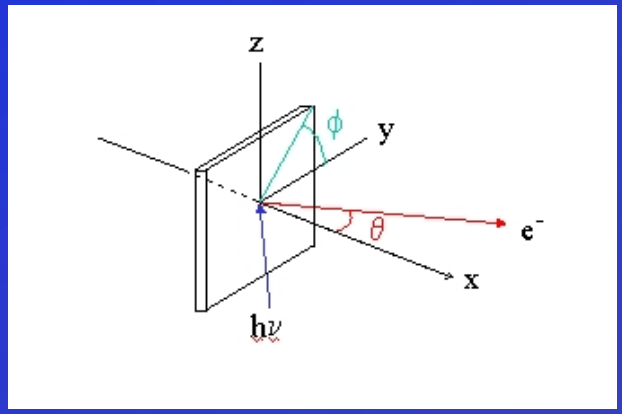

Measures the kinetic energy E_K and momentum $\mathbf{p}_{//}$ of electrons emitted from the surface of the film

Tringides, Jalochowski, Bauer,
Physics Today **60** (no 4), 50 (2007)

Quantum-size effects on surface reactivity: Mg films

Spectromicroscopy Experiment:

Aballe, Barinov, Locatelli, Heun, Kiskinova, PRL 93, 196103(2004); Aballe et al., J. Phys.: Cond. Matter 22, 015001 (2010)

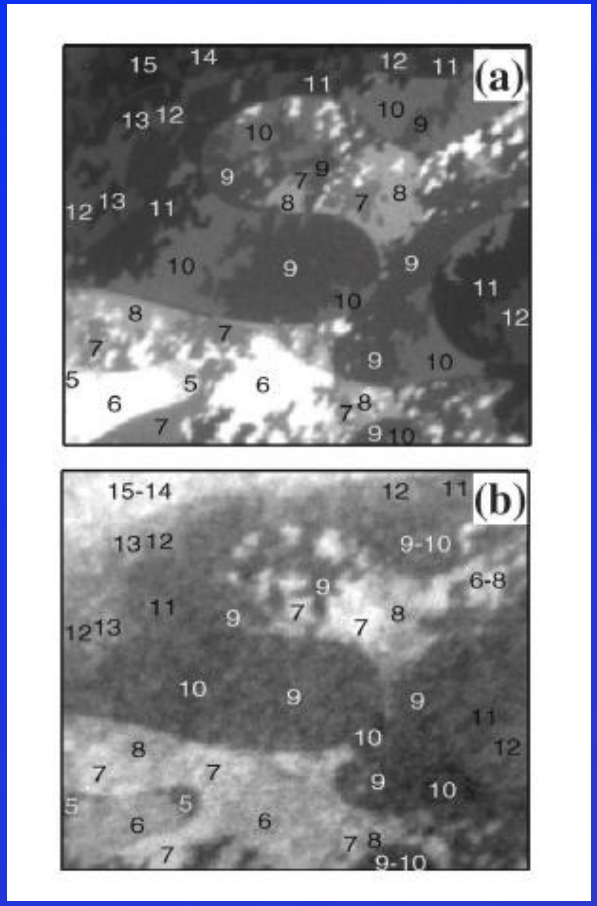

6 x 5 μm² images of a Mg (0001) film on W (110) with microregions of different Mg film thicknesses

(a) Before oxygen exposure

LEEM (Low-Energy Electron Microscopy)

Thickness determined from reflectivity changes

(b) After oxygen exposure

XPEEM (X-ray photoelectron Emission Microscopy)

Contrast corresponds to the extent of Mg oxidation (from the intensity of Mg 2p oxide component)

➢ **Modulation in the oxidation rate with Mg film thickness**

Quantum-size effects on surface reactivity: Mg films

Spectromicroscopy: Aballe et al. PRL 93, 196103(2004); J. Phys.: Cond. Matter 22, 015001 (2010)

Valence PE near normal emission ($k_{//} \approx 0$)

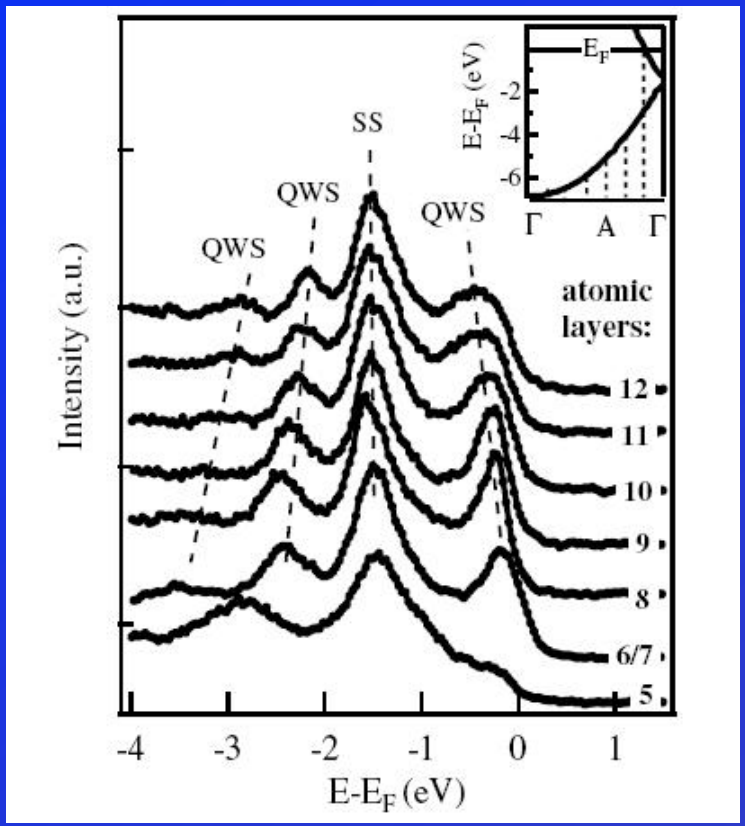

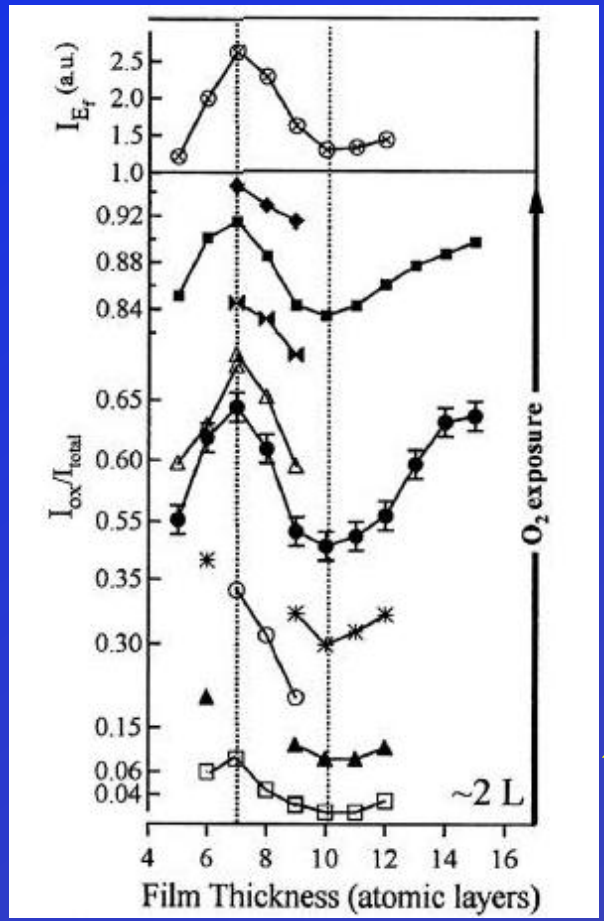

$I_{k_{//}\approx 0}(E_F)$

Oxidation rate (***from intensity of Mg 2p oxide component***)

Drastic (1-2 orders of magnitude) changes!

Origin of the correlation between surface reactivity and QWS ?

DFT calculations of Mg thin films on W(110)

Calculated DFT DOS versus measured normal-emission PE spectra

Partial DOS at $\mathbf{k}_{//} = \mathbf{0}$ PE by Aballe *et al.*

Mg(0001)/W

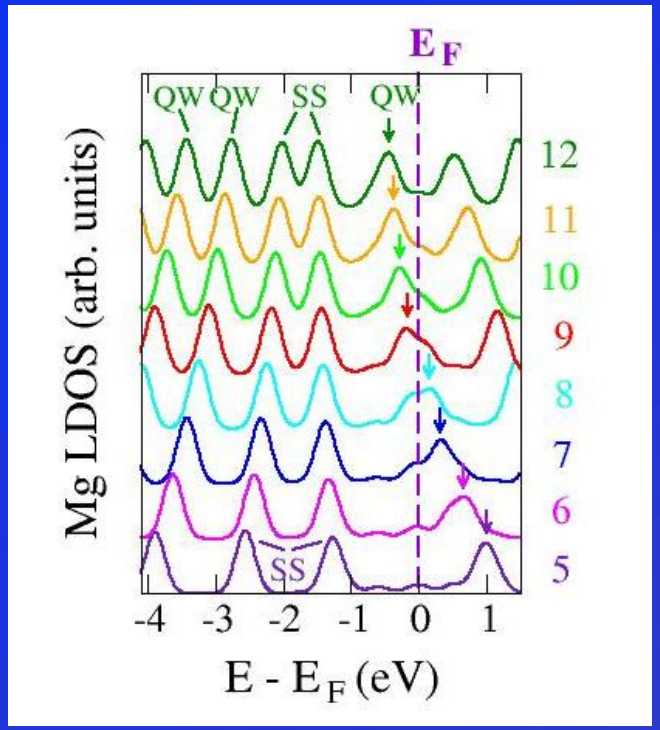

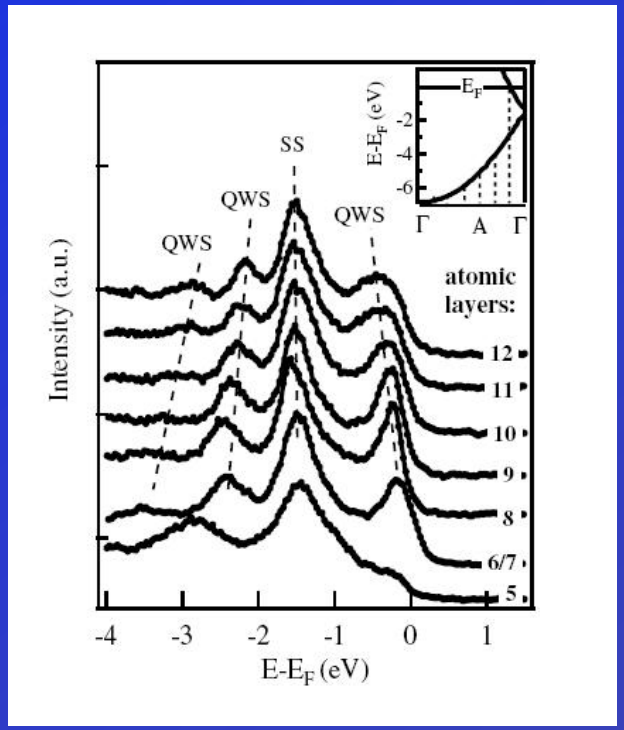

- Good general agreement in the peak positions

Binggeli and Altarelli, Phys. Rev. Lett. 96, 36805 (2006); Phys. Rev. B 78, 35438 (2008)

DFT calculations for Mg films on W(110)

- **Decay length in vacuum λ of the metal film electronic local density of states at E_F**

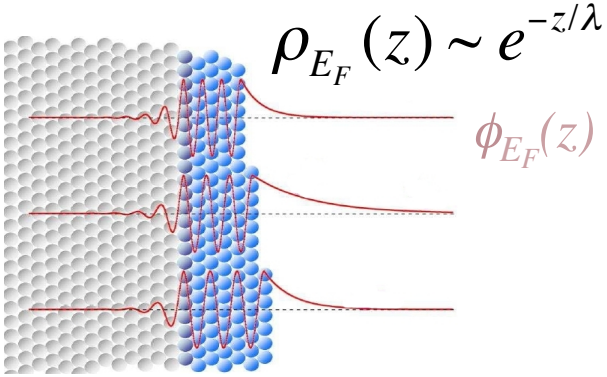

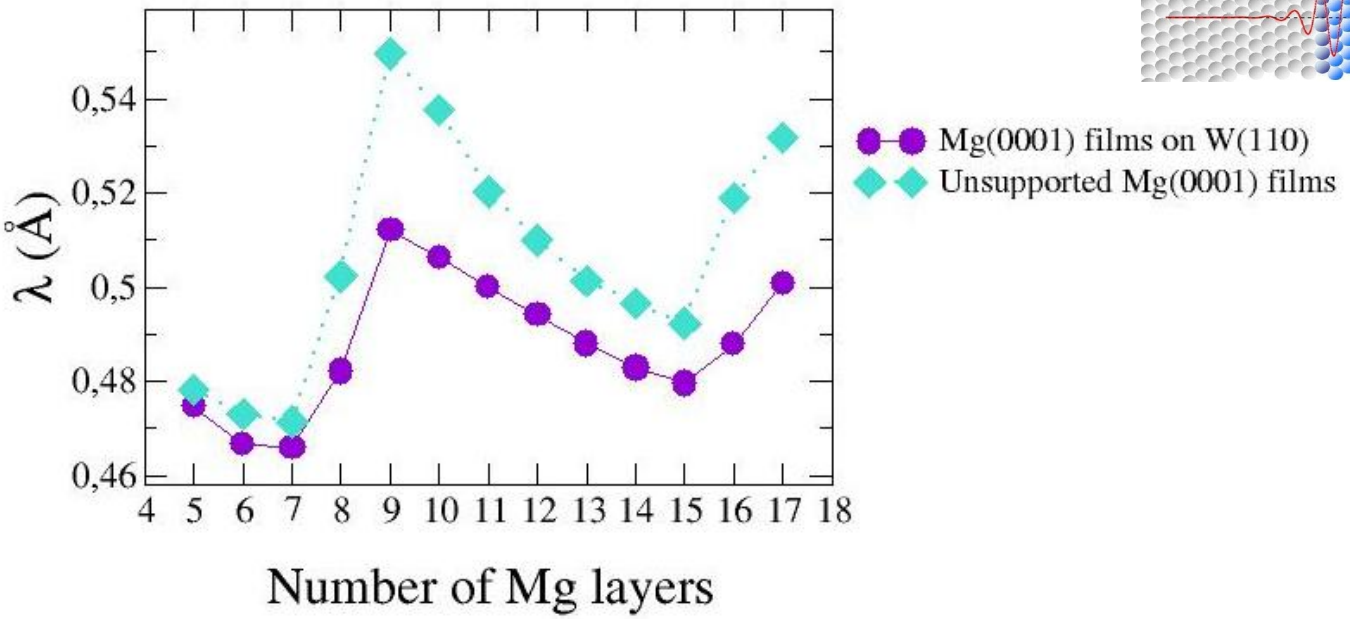

- ***Substantial oscillations in λ***

  substrate reduces the variation from 17% to 10 %

Binggeli and Altarelli, Phys. Rev. Lett. 96, 36805 (2006); Phys. Rev. B 78, 35438 (2008)

DFT calculations of Mg thin films on W(110)

Electronic decay length λ

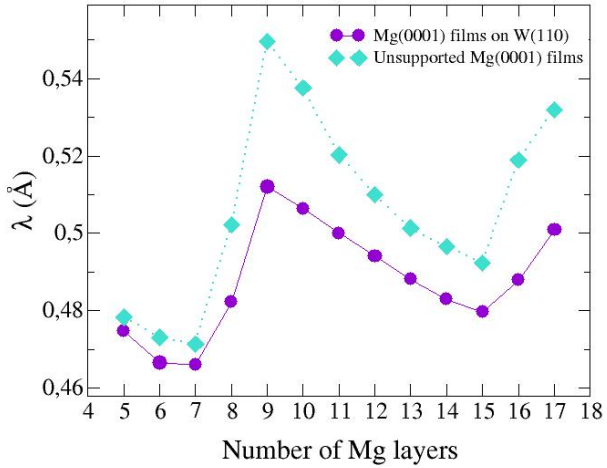

— Mg(0001) films on W(110)

◆ Free-standing Mg(0001) films

Partial density of states ($k_{//}$=0)

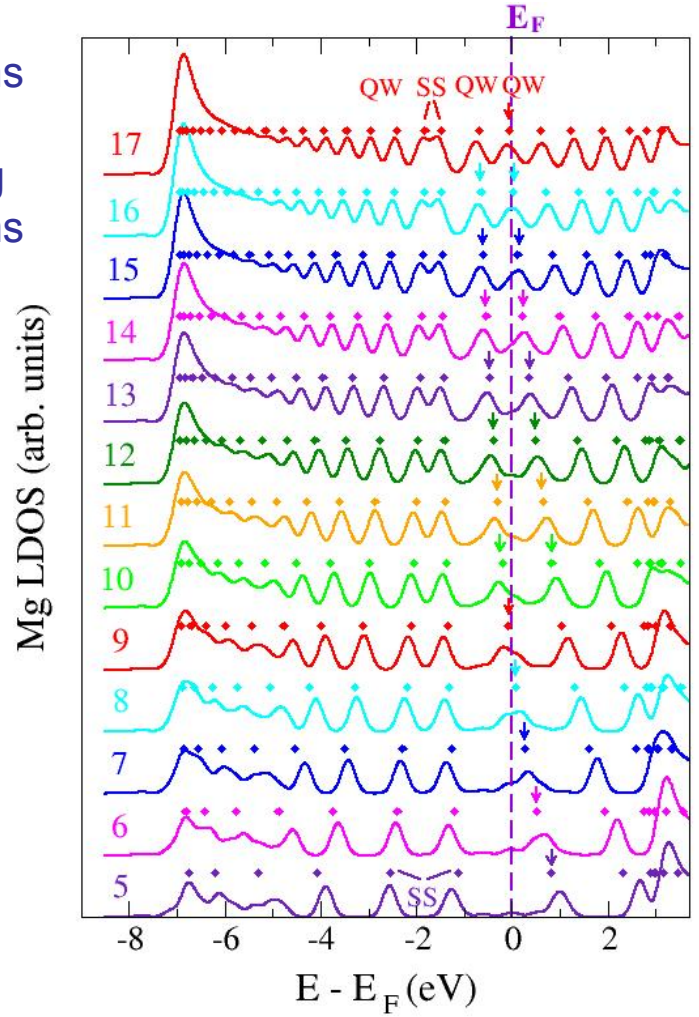

- ***λ is maximum when a Quantum-Well State (QWS) at $k_{//}$ = 0 crosses E_F***

trend explained by model description for λ

$$\lambda \sim 1/\sqrt{-E_M}$$

E_M : Energy of the highest occupied QW state at $K_{//}$ = 0 relative to the vacuum level

Binggeli and Altarelli, Phys. Rev. Lett. 96, 36805 (2006); Phys. Rev. B 78, 35438 (2008)

Origin of the changes in the surface reactivity ?

Binggeli and Altarelli, Phys. Rev. Lett. 96, 35805 (2006); Phys. Rev. B 78, 35438 (2008)

The changes in λ are expected to influence the electron transfer process from the O_2 molecule to the metal surface (by tunneling), which is believed to control the initial sticking of O_2 on the metal surface (via the attractive image charge potential on the ionized O_2^- molecule)

Hellman et al., Surface Science 532, 126 (2003).

The changes in λ are expected to have an exponential impact on the electron tunneling rate, and therefore on the initial sticking of O_2

A 10% change in λ will produce a 100% change in the transfer rate ~ $e^{-d/\lambda}$, at d ~3.5 Å, which is of the order of magnitude of the experimental change in the oxidation rate at low O_2 exposure

→ **Can explain the order of magnitude change observed experimentally**

Angle resolved photoemission spectra

Mg films on W(110)

8 ML **12 ML** **16 ML** **22 ML**

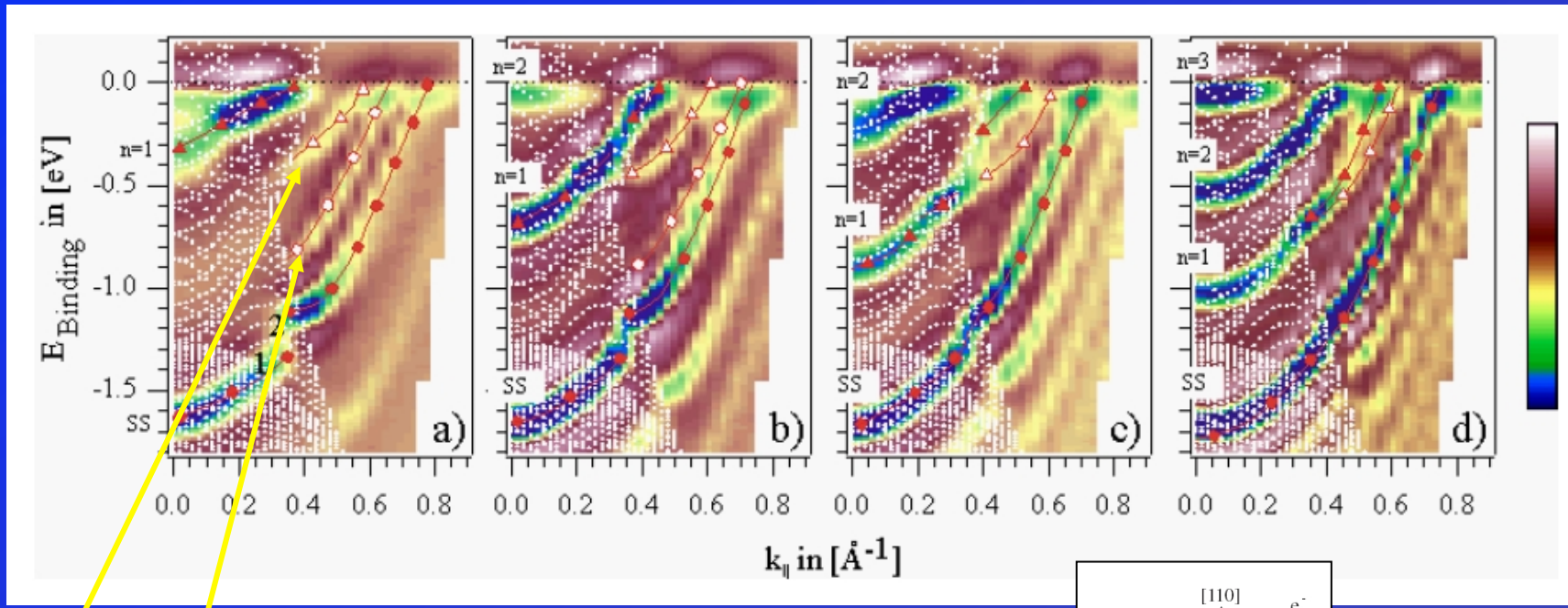

New (split) states

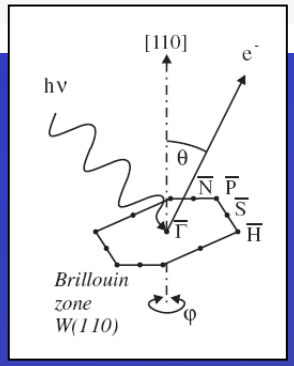

Koitzsch et al., Phys. Rev. Lett. **95**, 126401 (2005)

DFT results for Mg QWS:
8 Mg ML on W(110)

Binggeli and Altarelli, Phys. Rev. B **78**, 35438 (2008)

$K_{//}$ along the ΓS direction

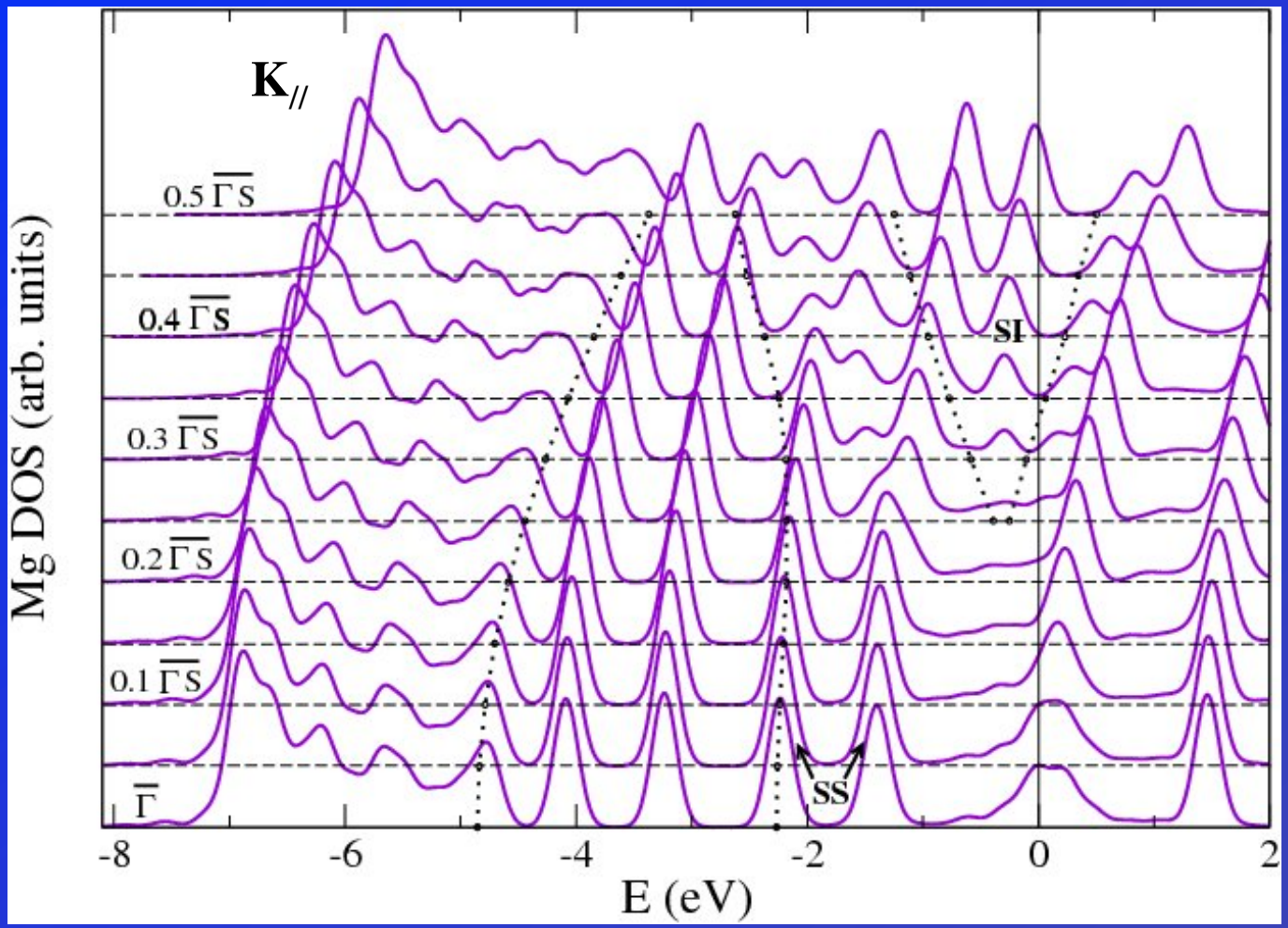

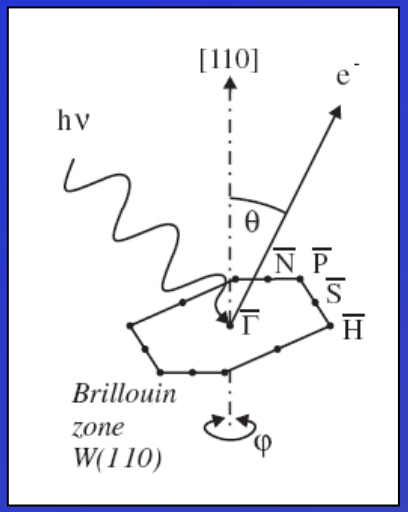

SI: These states result from the interaction of the Mg(0001) Shockley surface states with the W(110) surface state at the Interface

Resonant elastic x-ray scattering to probe orbital order in complex transition-metal coumpounds

(such as manganites)

- **Properties controlled** by a ***complex interplay*** between ***structural***, ***magnetic,*** and valence ***electronic charge/orbital*** degrees of freedom

Perovskite structure

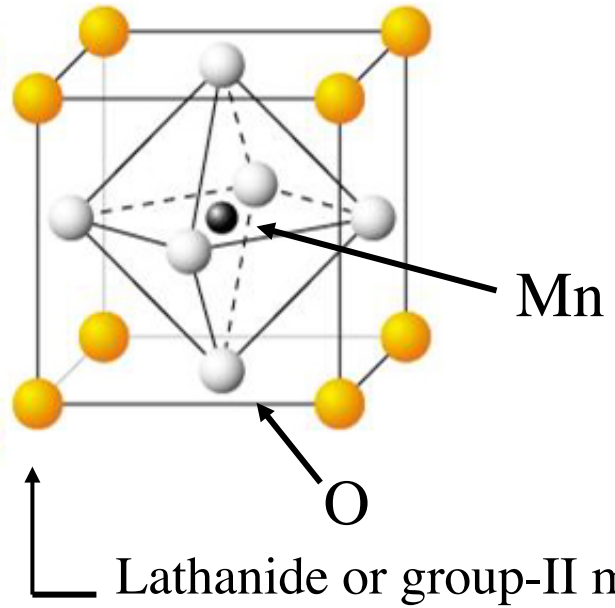

Layered Perovskite structures

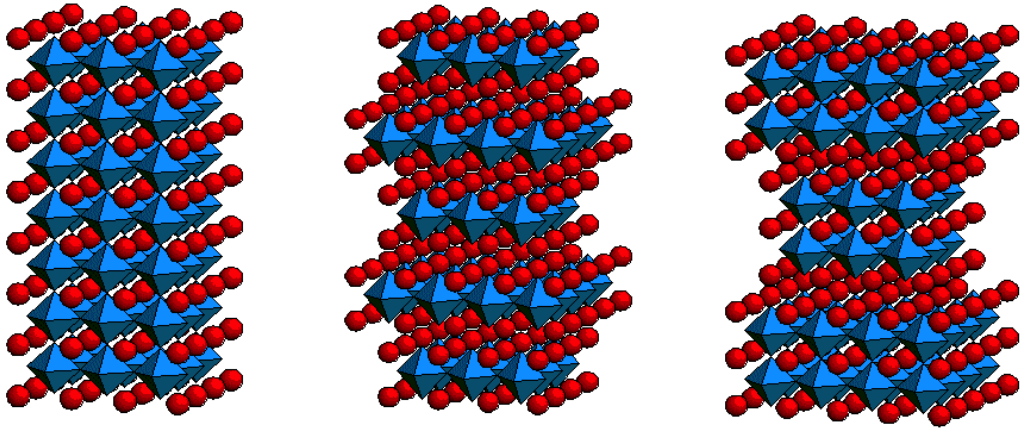

n = ∞
ABO_3
perovskite

n = 1
A_2BO_4
K_2NiF_4

n = 2
$A_3B_2O_7$
bilayer

Resonant elastic x-ray scattering to probe orbital order in complex transition-metal coumpounds

(such as manganites)

- **Properties controlled** by a ***complex interplay*** between ***structural***, ***magnetic,*** and valence ***electronic charge/orbital*** degrees of freedom

Orbital and spin ordering in perovskites

3d orbital degeneracy

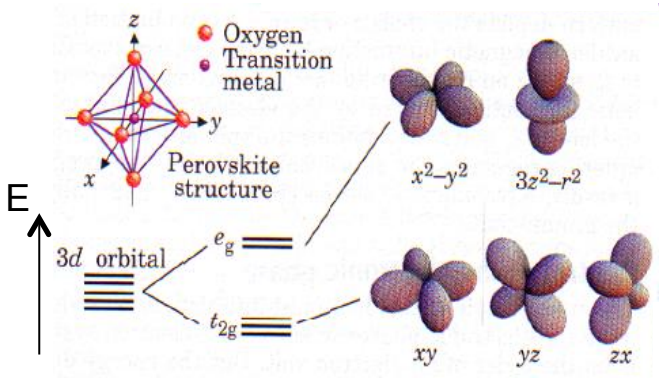

$LaVO_3$

V ($3d^2$)

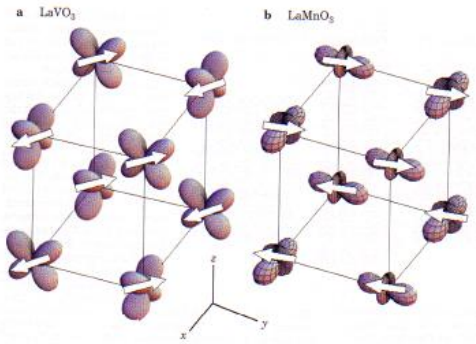

$LaMnO_3$

Mn ($3d^4$)

$La_{0.5}Sr_{0.5}MnO_3$ (Coherently strained)

Mn ($3d^{3.5}$)

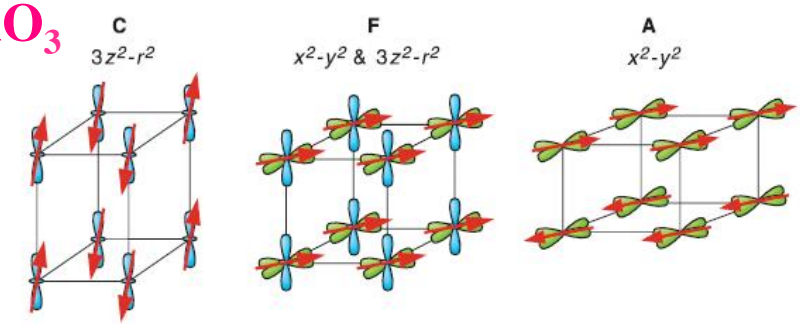

Tokura, Physics Today, 56 (7), 50 (2003)

The orbital order in complex transition-metal coumpounds

- ***The orbital degree of freedom*** of the 3d electrons plays a ***key role*** in the physics of manganites, but the orbital ordering is difficult to observe experimentally (***hidden to most experimental probes)***

- ***Resonant elastic X-ray Scattering*** (RXS) is a powerful ***tool to probe orbital ordering,*** but the interpretation of the experimental spectra is often controversial

→ ***importance of theoretical predictions***

Resonant elastic X-ray Scattering (RXS)

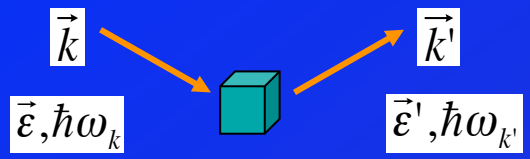

$|\vec{k}| = |\vec{k}'|$

Elastic scattering

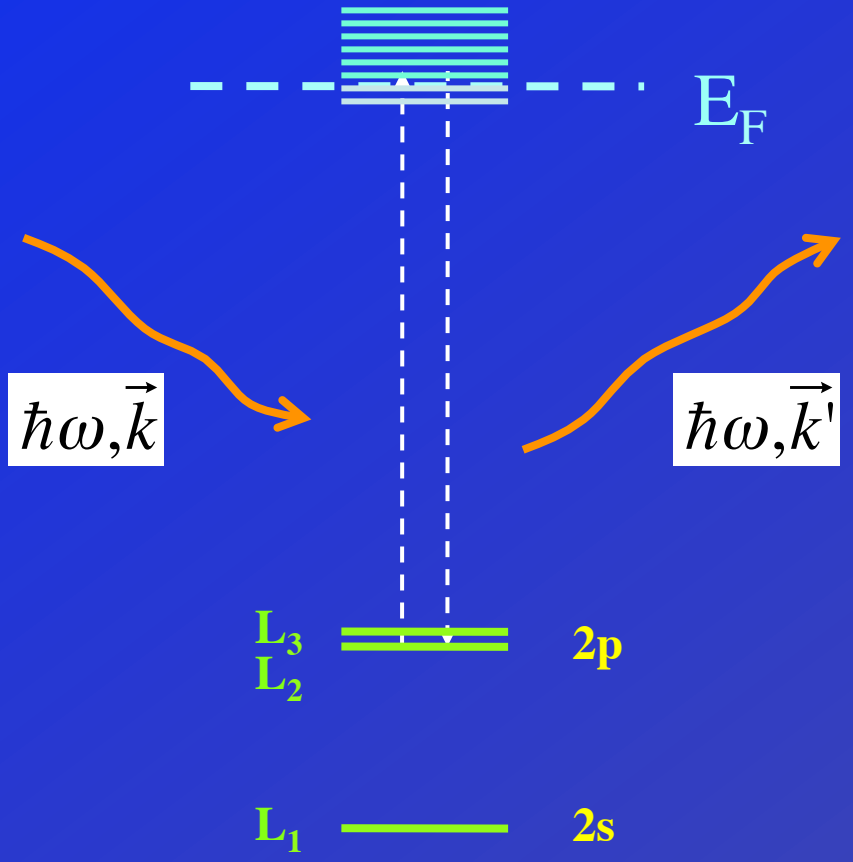

Photon energy resonant with a core level absorption edge

Resonant elastic x-ray scattering is a second order process in which a core electron is virtually promoted to some intermediate states above the Fermi energy, and subsequently decays to the same core level

Resonant elastic x-ray scattering

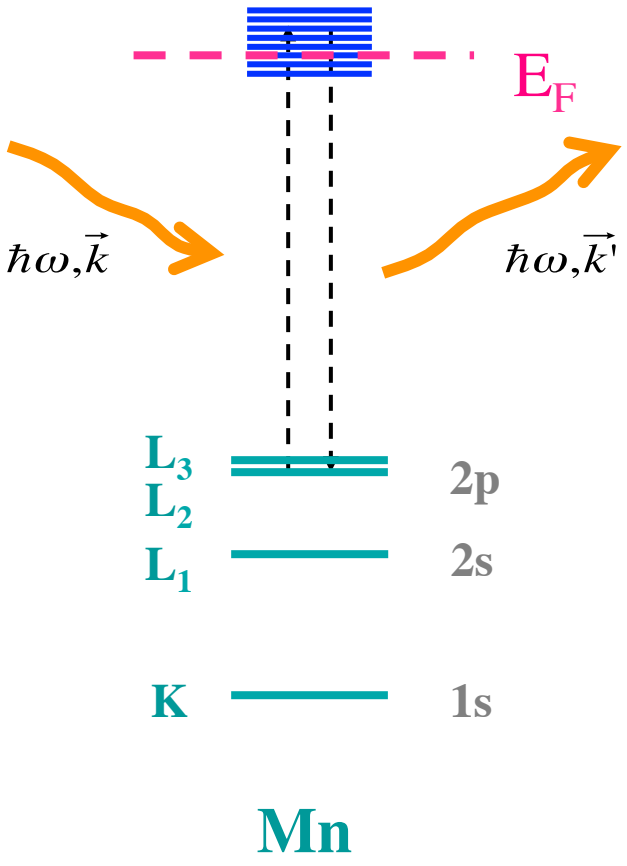

- **Scattering** for Bragg condition:

$$\vec{k} - \vec{k}' = \vec{G}_{lmn},$$

$\vec{G}_{lmn}$: reciprocal lattice (Bragg) vector

- **Resonant** scattering amplitude:

$$f(\vec{G},\hbar\omega) \propto \sum_{I(ions)} e^{i\vec{G}\vec{d}_I} \sum_{\alpha,\beta} F^I_{\alpha,\beta}(\hbar\omega)\varepsilon_\alpha\varepsilon'_\beta$$

$$F^I_{\alpha,\beta}(\hbar\omega) \propto \sum_n \frac{<0|R_\alpha(I)|n><n|R_\beta(I)|0>}{\hbar\omega + E_0 - E_n - i\Gamma/2}$$

- **selective probe of order/periodicity**
- **element sensitive**
- **photon-energy dependent**

- *At $L_{2,3}$ edge, in principle **orbital-order sensitive** (optical selection rule)*

Resonant x-ray scattering to probe orbital order in $KCuF_3$?

Crystal structure:

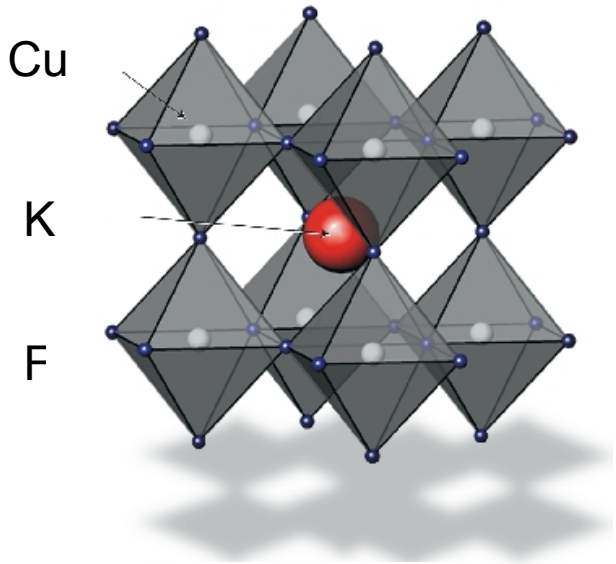

Jahn-Teller distortion

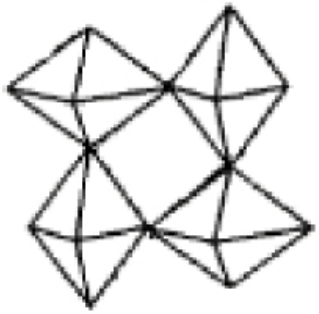

RXS at the Cu K edge in $KCuF_3$

Cu 1s -> 4p dipole transitions

Exp.: Paolasini et al., PRL 88, 106403 (2002); Caciuffo et al., PRB 65, 174425 (2002)

- pseudo cubic perovskite
- cooperative Jahn-Teller distortion below 1000 K
- *Neel* temperature ~38 K
- $d_{x^2-y^2}$ hole antiferroorbital ordering

Resonant x-ray scattering to probe orbital order in $KCuF_3$?

Crystal structure and OO:

Cu $3d^9$

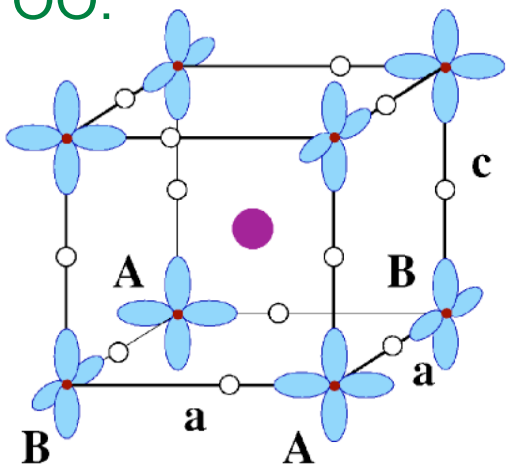

Jahn-Teller distortion

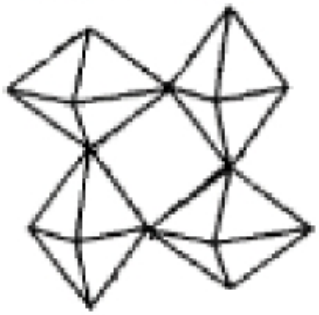

RXS at the Cu K edge in $KCuF_3$

Cu 1s -> 4p dipole transitions

Exp.: Paolasini et al., PRL 88, 106403 (2002); Caciuffo et al., PRB 65, 174425 (2002)

- pseudo cubic perovskite
- cooperative Jahn-Teller distortion below 1000 K
- *Neel* temperature ~38 K
- $d_{x^2-y^2}$ hole antiferroorbital ordering

Resonant x-ray scattering to probe orbital order in $KCuF_3$?

$KCuF_3$

Cu $3d^9$

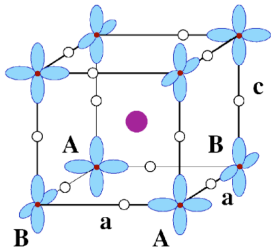

Jahn-Teller distortion

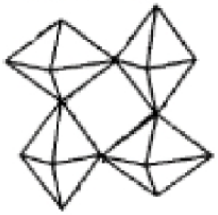

LDA+U

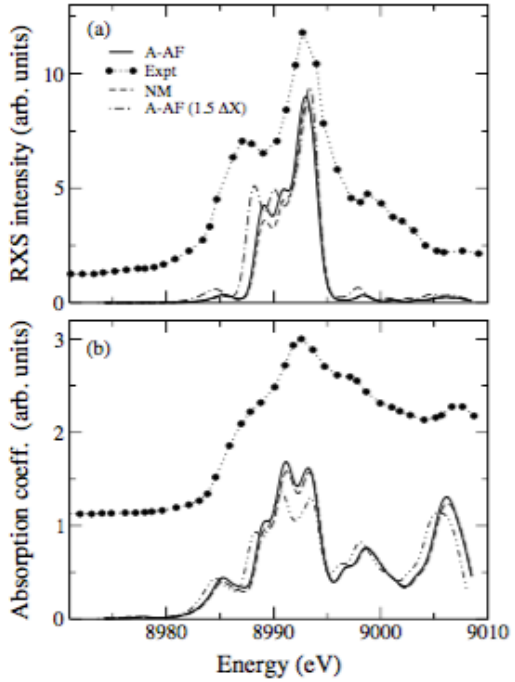

FIG. 9: Orbital RXS intensity (a) and absorption coefficient (b), as a function of photon energy, near the Cu K edge in $KCuF_3$. The calculated spectra of the A-AF (solid line) and NM (dashed line) structures are displayed. The effect of a 50 % increase in the quadrupolar distortion, ΔX, in the A-AF structure is also shown (dashed-dotted line). The experimental data are from Ref. 7; the measured RXS spectrum corresponds to a (3,3,1) orbital Bragg reflection and a $\sigma - \pi'$ polarization.

Cu K-edge:
1s -> 4p dipole transitions

Atomic resonant scattering amplitude

$$F^j_{\alpha,\beta}(\hbar\omega) = \sum_{\boldsymbol{k},n} \frac{\langle\psi_0^{(j)}|r_\alpha(j)|\psi^{4p}_{\boldsymbol{k},n}\rangle\langle\psi^{4p}_{\boldsymbol{k},n}|r_\beta(j)|\psi_0^{(j)}\rangle}{\hbar\omega + E_0 - E^{4p}_{\boldsymbol{k},n} - i\Gamma/2}$$

RXS intensity

$$I(\boldsymbol{G},\hbar\omega) \propto \left|\sum_j e^{i\boldsymbol{Q}\cdot\boldsymbol{R}_j} \sum_{\alpha,\beta} F^j_{\alpha,\beta}(\hbar\omega)\epsilon_\alpha\epsilon'_\beta\right|^2$$

with $\vec{G} = \vec{Q}_{OO}$

$$I_{\rm orb}(\hbar\omega) \propto \left|F^A_{x,x}(\hbar\omega) - F^A_{y,y}(\hbar\omega)\right|^2$$

For Orbital Ordering

Absorption

$$A(\hbar\omega) \propto Im[F^A_{x,x}(\hbar\omega) + F^A_{y,y}(\hbar\omega) + F^A_{z,z}(\hbar\omega)]$$

- Good general agreement with exp.
- RXS: controlled by Jahn-Teller distortion
  not sensitive to OO
  not sensitive to spin order

Binggeli and Altarelli , Phys. Rev. B 70, 085117 (2004)

Resonant elastic x-ray scattering to probe orbital order in manganites ?

RXS at the Mn $L_{2,3}$ edges in manganites (L_2:$2p_{1/2}$, L_3:$2p_{3/2}$)

Mn 2p -> 3d dipole transitions

Exp.: Wilkins, Spencer, Hatton *et al.*, PRL **91**, 167205 (2003)

$La_{0.5}Sr_{1.5}MnO_4$

Crystal structure

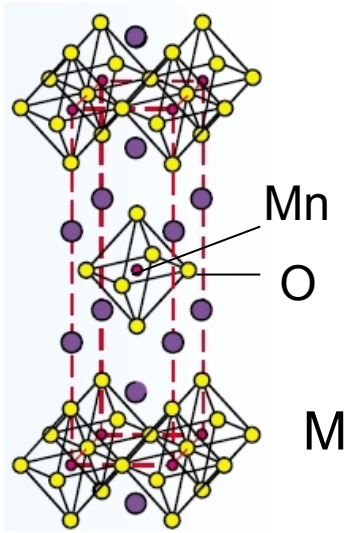

Mn-3d charge and orbital order

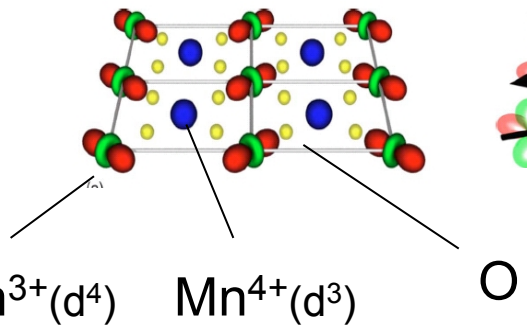

Magnetic order

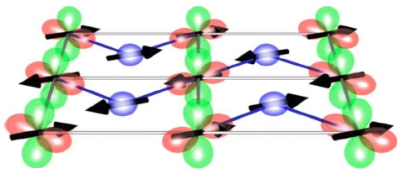

$L_{2,3}$ absorption edge

Multiplet effects in XAS, RXS

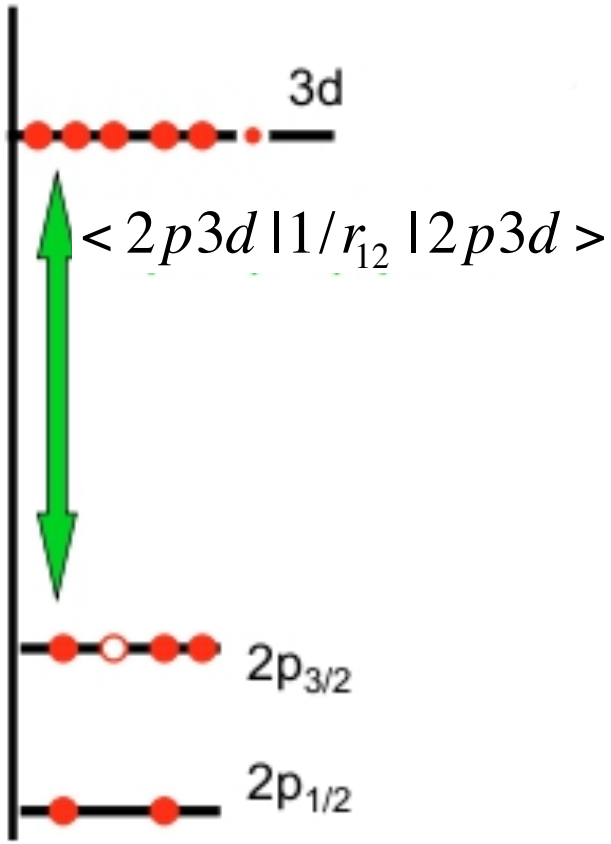

Strong overlap of core and valence wave functions

2p -> 3d dipole transitions

$< 2p3d \,|1/r_{12}|\, 2p3d >$ Coulomb interaction terms cannot be neglected

Single particle picture breaks down!

Resonant x-ray scattering at the Mn $L_{2,3}$ edges in $La_{0.5}Sr_{1.5}MnO_4$

$La_{0.5}Sr_{1.5}MnO_4$

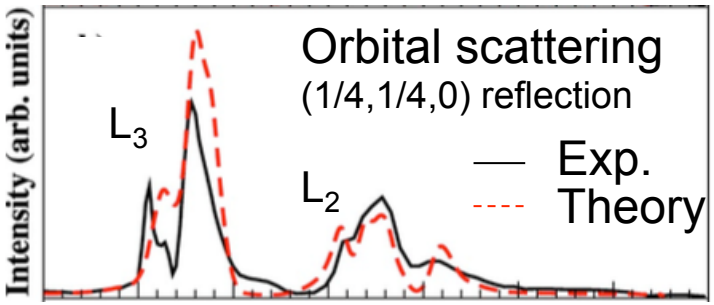

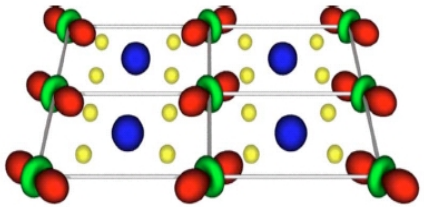

Wilkins, Stojic, Beale, Binggeli *et al.,* Phys. Rev. B 71, 245102 (2005); J. Phys. Condens. Matter 18, L323 (2006).

Mn^{3+} atomic multiplet calculations in a crystal field

- Good general agreement with experiment
- RXS sensitive to OO and Jahn-Teller distortion

Nanostructured Graphene

on Ir(001) surface

Temperature-driven reversible rippling and bonding of a graphene superlattice
A. Locatelli, C. Wang, C. Africh, N. Stojic, T. O. Mentes, G. Comelli, and N. Binggeli, *ACS Nano* **7**, 6955 (2013)

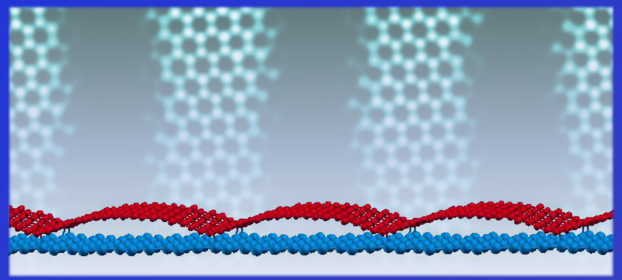

Nanobubbles at GPa Pressure under Graphene
G. Zamborlini, M. Imam, L. L. Patera, T. O. Mentes, N. Stojic, C. Africh, A. Sala, N. Binggeli, G. Comelli, and A. Locatelli, *Nano Lett*. ***15***, *6162 (2015)*

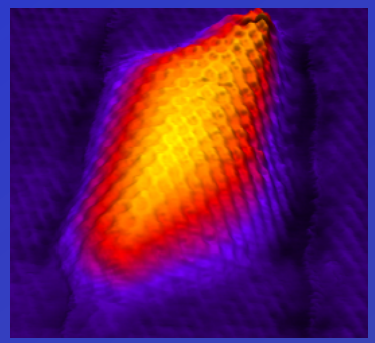

Graphene nanobuckled phase on Ir(001)

LEEM/
LEED

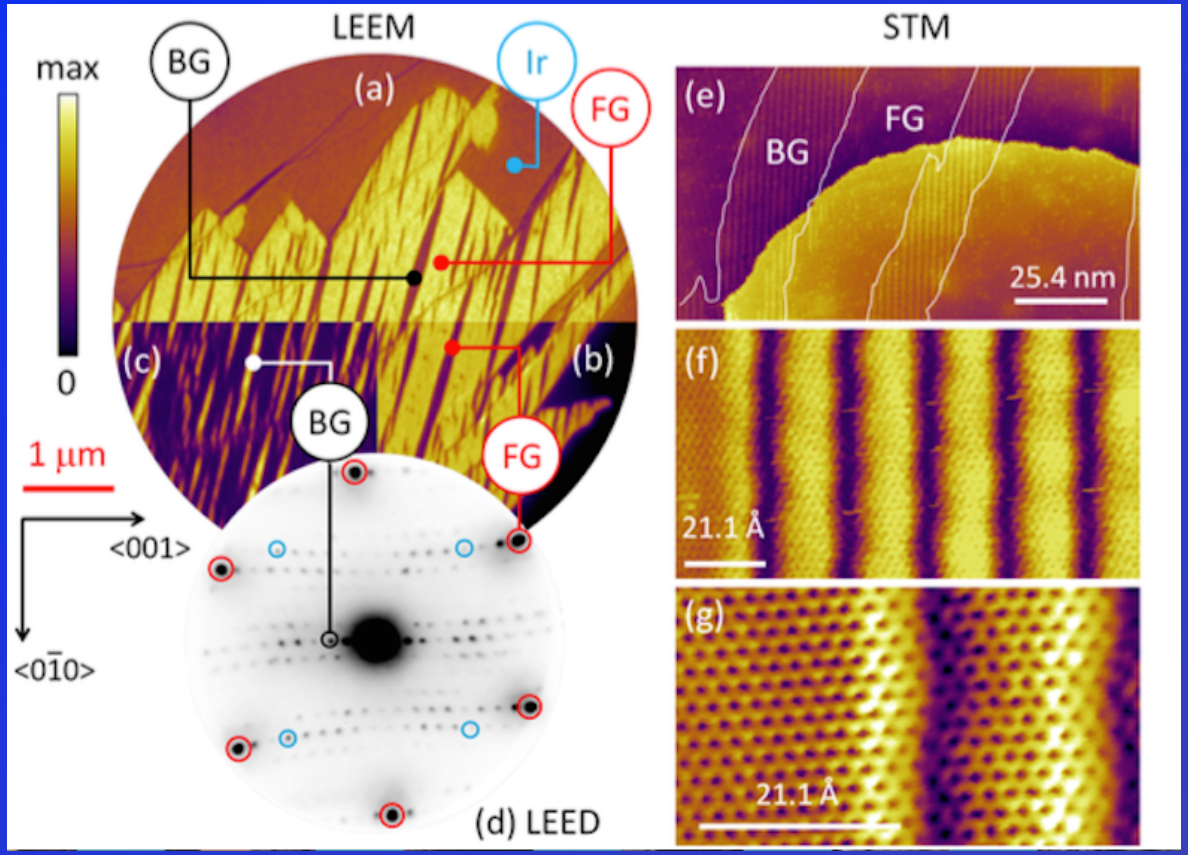

STM

On Ir substrate: Buckled phase of Graphene with exceptionally large one-dimensional ripples with regular nanometer periodicity

A. Locatelli, C. Wang, C. Africh, N. Stojic, T. O. Mentes, G. Comelli, and N. Binggeli, *ACS Nano* **7**, 6955 (2013)

Graphene nanobuckled phase on Ir(001)

Gr/Ir DFT **isolated Gr**

Top view

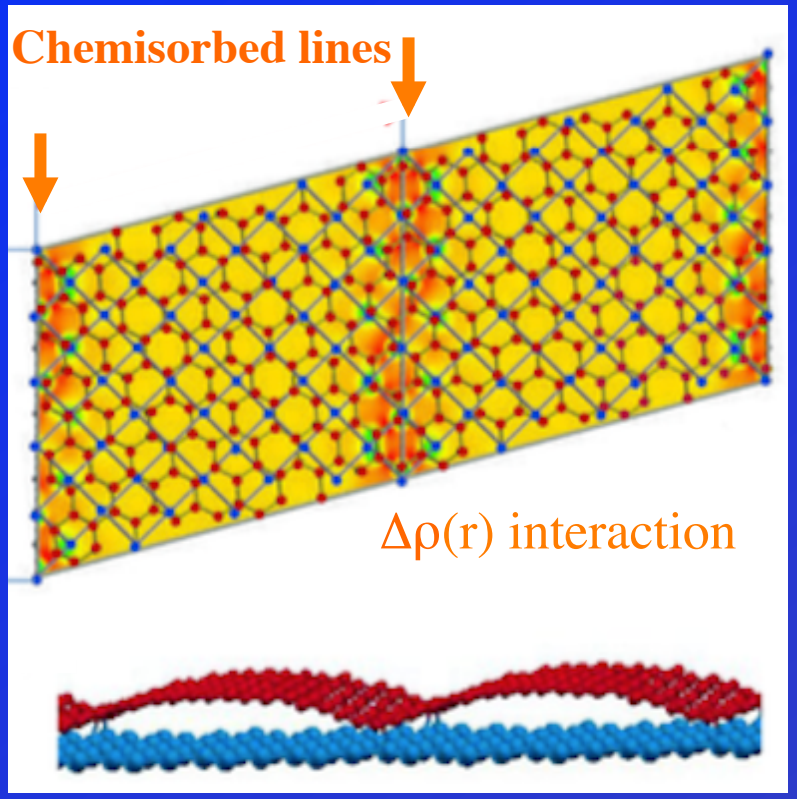

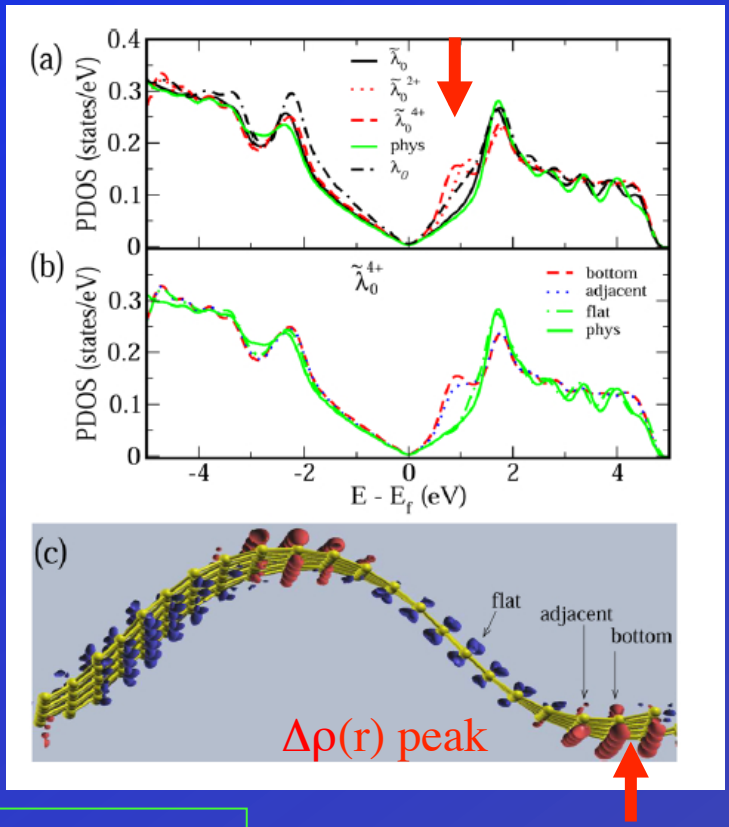

DOS bottom C rows

Side view

- Chemisorbed line includes ~ 3 rows of C
- BG curvature induces a C-2p_z DOS feature near E_F
- the corresponding states are found to be largely responsible for strong local chemisorption

M. Imam, N. Stojic, and N. Binggeli, *J. Phys. Chem.* C, **118**, 9514 (2014)

Graphene nanobuckled phase on Ir(001)

DFT

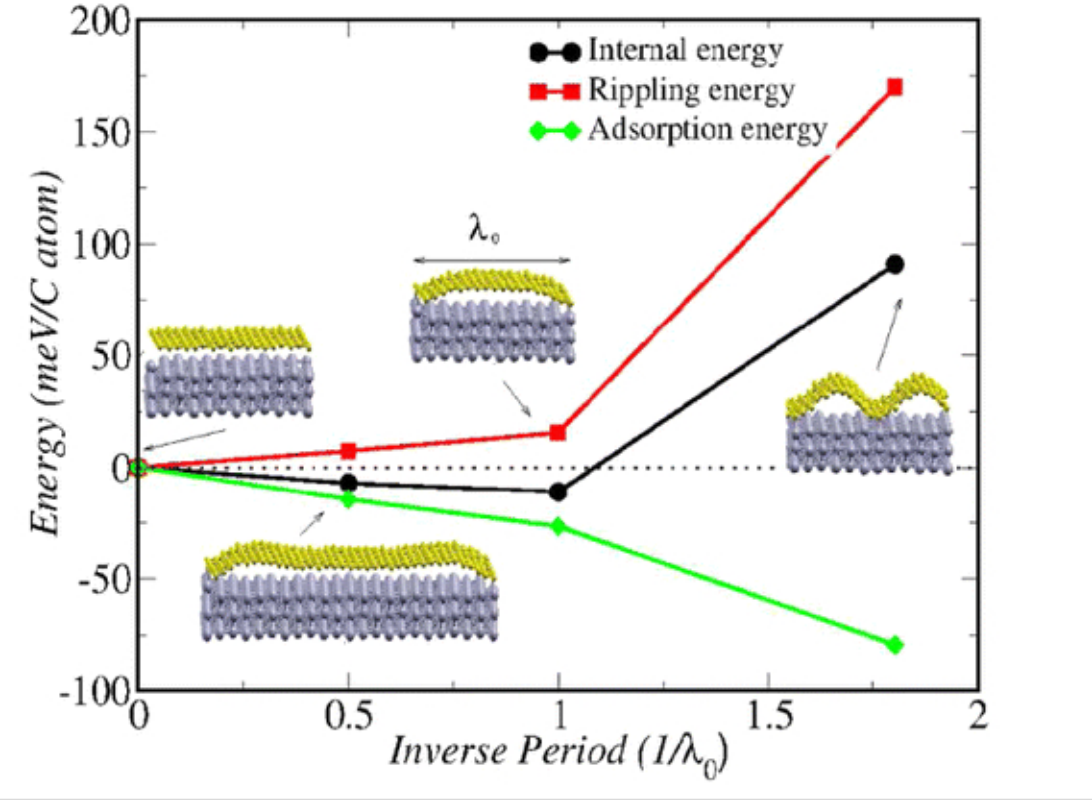

The nm periodicity is explained by the trends of the rippling and chemisorption energy

The nm period is related to the onset of the non-linear behavior of the rippling energy - which overcomes the chemisorption energy at short period

M. Imam, N. Stojic, and N. Binggeli, *J. Phys. Chem.* C, **118**, 9514 (2014)

Graphene nanobubbles on Ir(001)

Nanospectroscopy group @ Elettra:

Upon irradiation with Ar^+ ions (sputt. 0.1-0.4 kV) and subsequent annealing T: 80 C, ...,1080 C

STM @ CNR-IOM TASC

Trapped Ar

Ripening with T

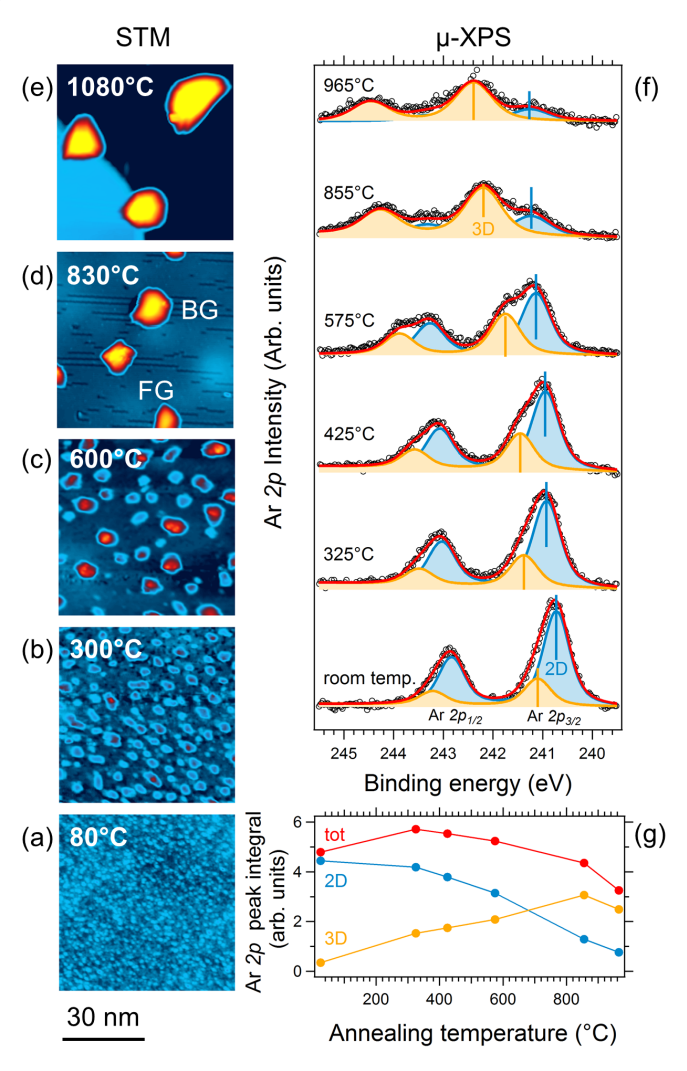

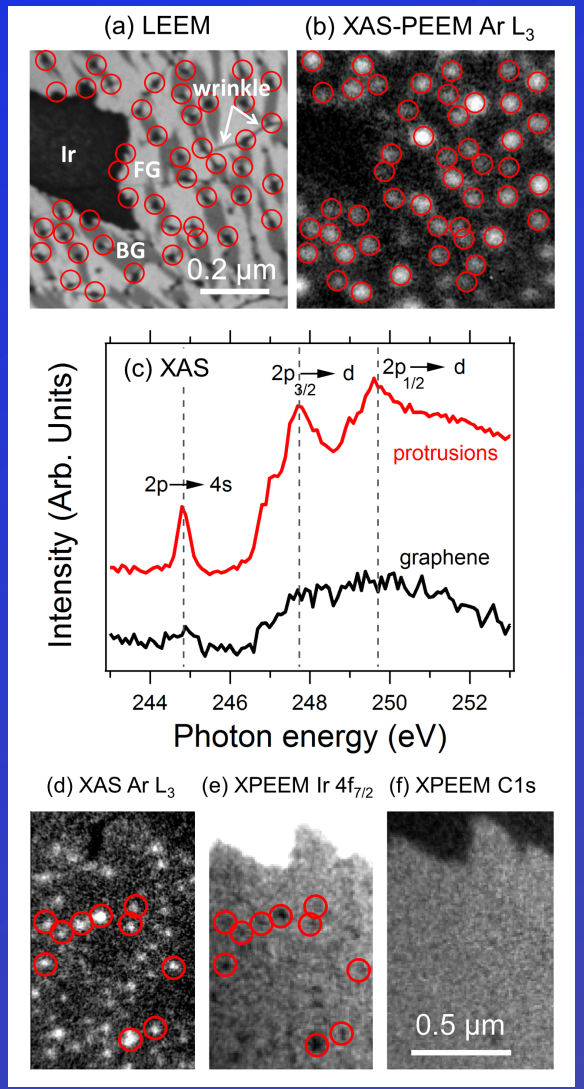

Zamborlini et al. *Nano Lett.* **15**, 6162 (2015)

Graphene nanobubbles on Ir(001)

DFT

Equilibrium configurations

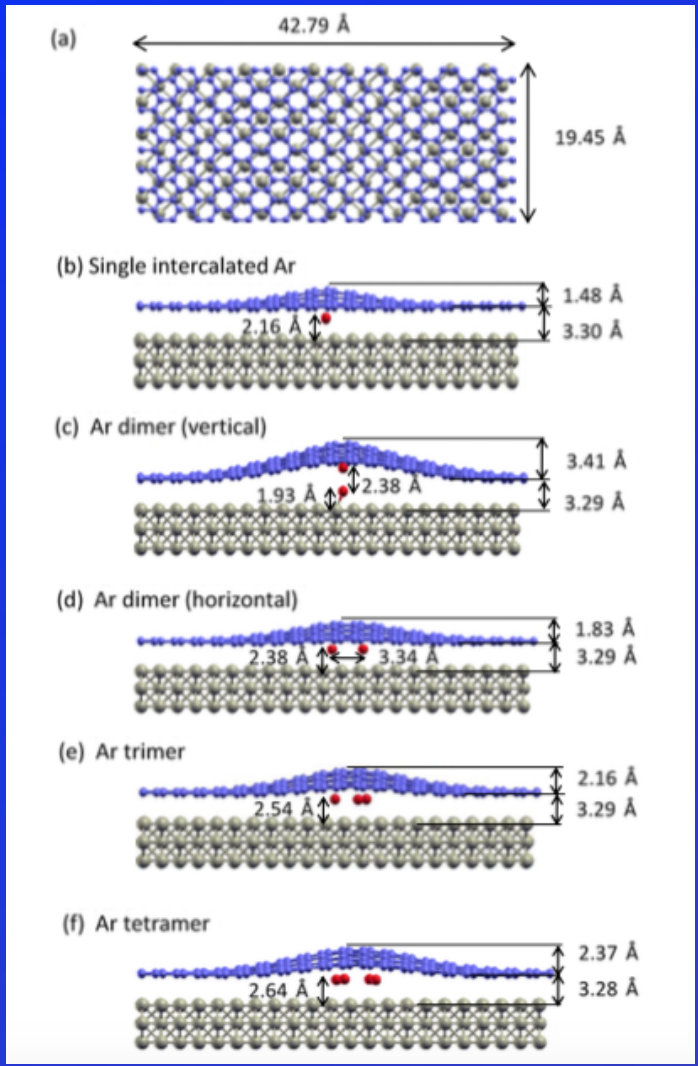

The Ar-Ar bond in intercalated cluster is strongly contracted with respect to bulk Ar (3.82 Å) or Ar dimer in vac. (3.74 Å)

The corresponding effective pressure experienced by intercalated Ar cluster is in the GPa range (8-25 GPa)

G. Zamborlini, M. Imam et al. *Nano Lett.* ***15***, *6162 (2015)*

Graphene nanobubbles on Ir(001)

Ar cluster formation energy:

$\Delta E = E^{NAr} - N\,E^{1Ar}$

G. Zamborlini, M. Imam* et al.
Nano Lett. ***15***, *6162 (2015)*

* *Computations by Mighfar Imam*

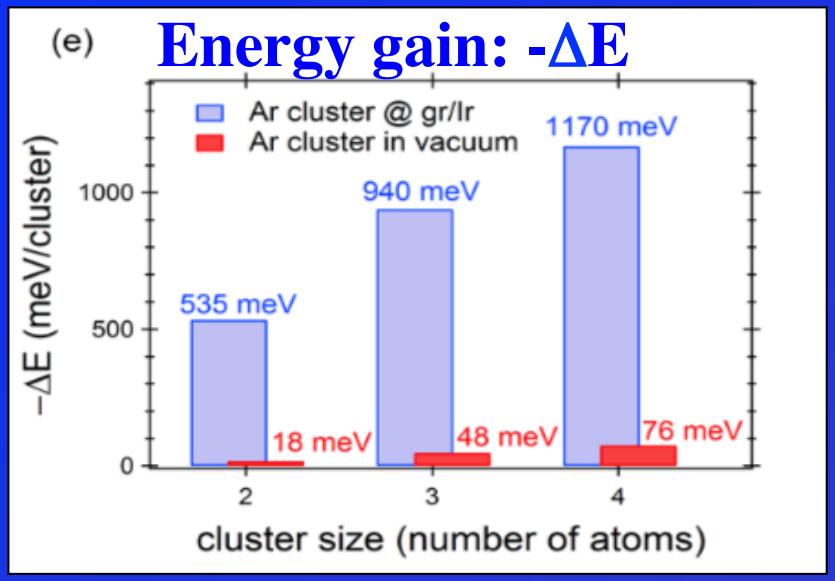

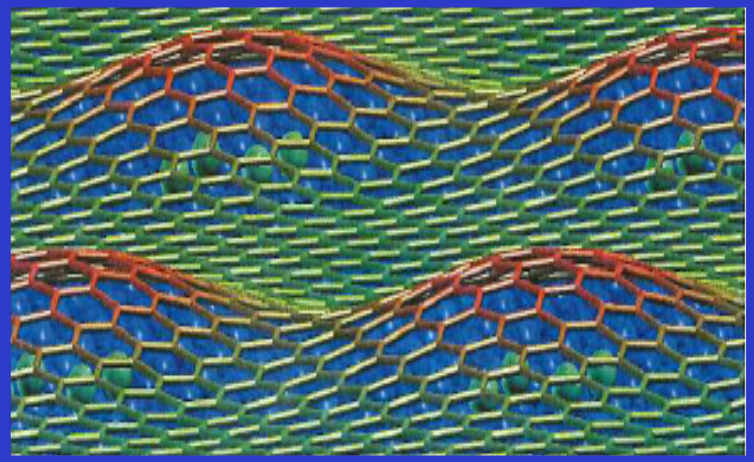

- Drastic increase in the energy gain for Ar cluster formation at the Gr/Ir interface (compared to Ar cluster in vacuum), related to the distortion of the physisorbed graphene
- Major gain in energy when two or more bubbles merge into a single one
- The bubble formation is driven by minimization of the energy cost of membrane distortion and loss of adhesion